

# Multi-Center Magnon Excitations Open the Entire Brillouin Zone to Terahertz Magnetometry of Quantum Magnets

Tobias Biesner, Seulki Roh, Aleksandar Razpopov, Jannis Willwater, Stefan Süllow, Ying Li, Katharina M. Zoch, Marisa Medarde, Jürgen Nuss, Denis Gorbunov, Yurii Skourski, Andrej Pustogow, Stuart E. Brown, Cornelius Krellner, Roser Valentí,\* Pascal Puphal,\* and Martin Dressel\*

Due to the small photon momentum, optical spectroscopy commonly probes magnetic excitations only at the center of the Brillouin zone; however, there are ways to override this restriction. In case of the distorted kagome quantum magnet Y-kapellasite,  $Y_3Cu_9(OH)_{19}Cl_8$ , under scrutiny here, the spin (magnon) density of states (SDOS) can be accessed over the entire Brillouin zone through three-center magnon excitations. This mechanism is aided by the three different magnetic sublattices and strong short-range correlations in the distorted kagome lattice. The results of THz time-domain experiments agree remarkably well with linear spin-wave theory (LSWT). Relaxing the conventional zone-center constraint of photons gives a new aspect to probe magnetism in matter.

## 1. Introduction

Conservations of momentum and energy are fundamental principles in physics that have to be obeyed also by optical excitations in solids. In an isolated system, for example, direct electronic transitions induced by light follow both  $\Delta E = E_{ph}$  and  $\Delta q = q_{ph}$ , where  $\Delta E$  and  $\Delta q$  are the energy and momentum differences between the initial and the excited states, respectively, while  $E_{ph}$  and  $q_{ph}$  are energy and momentum of the photon.<sup>[1,2]</sup> By the same token, these two principles dictate magnetic excitations as well. Here, a magnon with momentum

T. Biesner, S. Roh, A. Pustogow, M. Dressel  
1. Physikalisches Institut  
Universität Stuttgart  
70550 Stuttgart, Germany  
E-mail: dressel@pi1.physik.uni-stuttgart.de

A. Razpopov, Y. Li, R. Valentí  
Institut für Theoretische Physik  
Goethe-Universität Frankfurt  
60438 Frankfurt am Main, Germany  
E-mail: valenti@itp.uni-frankfurt.de

J. Willwater, S. Süllow  
Institut für Physik der Kondensierten Materie  
Technische Universität Braunschweig  
38106 Braunschweig, Germany

Y. Li  
Department of Applied Physics and MOE Key Laboratory for Nonequilibrium Synthesis and Modulation of Condensed Matter  
School of Physics  
Xi'an Jiaotong University  
Xi'an 710049, China

K. M. Zoch, C. Krellner, P. Puphal  
Physikalisches Institut  
Goethe-Universität Frankfurt  
60438 Frankfurt am Main, Germany  
E-mail: p.puphal@fkf.mpg.de


M. Medarde, P. Puphal  
Laboratory for Multiscale Materials Experiments  
Paul Scherrer Institute  
Villigen PSI 5232, Switzerland

J. Nuss, P. Puphal  
Max Planck Institute for Solid State Research  
70569 Stuttgart, Germany

D. Gorbunov, Y. Skourski  
Hochfeld-Magnetlabor Dresden (HLD-EMFL)  
Helmholtz-Zentrum Dresden-Rossendorf  
01328 Dresden, Germany

A. Pustogow, S. E. Brown  
Department of Physics and Astronomy  
UCLA  
Los Angeles, CA 90095, USA

A. Pustogow  
Institute of Solid State Physics  
TU Wien  
Vienna 1040, Austria

 The ORCID identification number(s) for the author(s) of this article can be found under <https://doi.org/10.1002/qute.202200023>

© 2022 The Authors. Advanced Quantum Technologies published by Wiley-VCH GmbH. This is an open access article under the terms of the Creative Commons Attribution License, which permits use, distribution and reproduction in any medium, provided the original work is properly cited.

DOI: 10.1002/qute.202200023

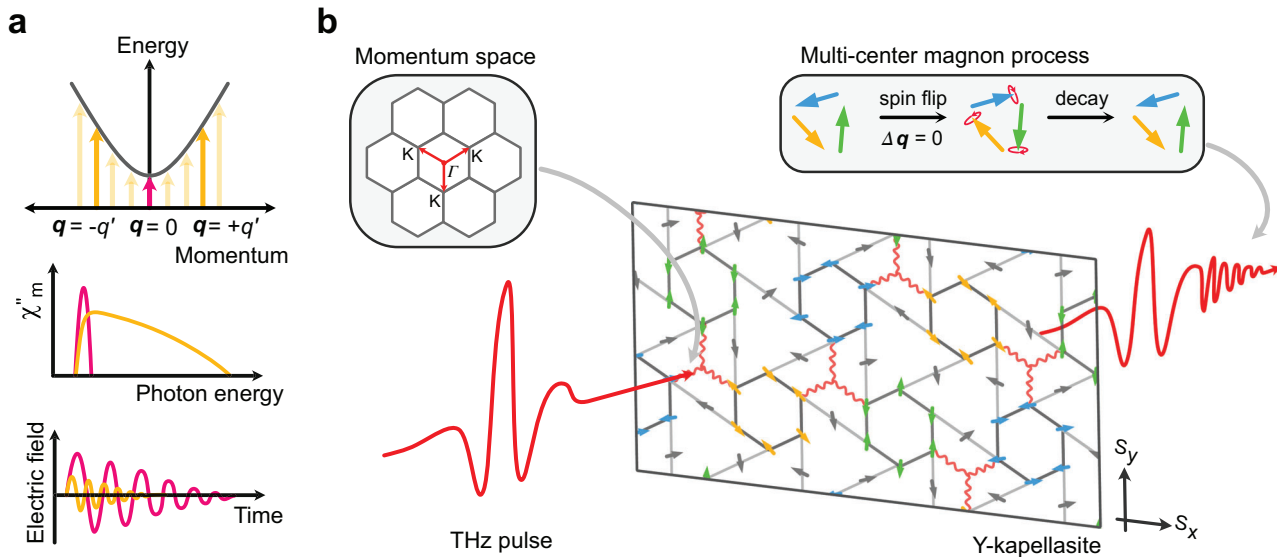


**Figure 1.** Three-center magnon process in Y-kapellasite. a) Comparison between the one-magnon (red) and two-center magnon absorption (yellow). The top panel describes the excitations in the spin-wave dispersion curve. While the one-magnon excitation only takes place near the zone center ( $q \approx 0$ ), the two-center magnon excitations can extend over the entire Brillouin zone ( $\Delta q \approx 0$  excitation). Here, the summed momenta of the participating magnons need to vanish,  $0 \approx \sum_n q_n$ , to ensure momentum conservation. The middle and bottom panel show the corresponding response in energy / frequency-dependent magnetic susceptibility  $\chi''_m$  and electric field as a function of time, respectively. A one-magnon excitation shows a sharp peak in  $\chi''_m$ , due to comparably long lifetimes (20–40 ps). A multi-center magnon excitation, however, is restricted to shorter time scales, correlated with a broad, continuum-like feature in  $\chi''_m$ . b) Schematics of three-center magnon absorption in Y-kapellasite and calculated ground state,  $\mathbf{Q} = (1/3, 1/3)$ . The simultaneous magnetic absorption occurs through three different magnetic sublattices (green, blue, and yellow hexagons in real space). The excited spin waves fall back to the initial state via a free induction decay resulting in oscillations of the outgoing THz pulse at extended time.

$q$  is created / annihilated by absorbing / emitting a photon. Within the energy conservation limit, the small photon momentum confines possible excitations close to the center of the Brillouin zone, that is,  $q \approx 0$ , due to its sharp energy–momentum dispersion ( $\omega = q_{\text{ph}} c_0 / n$ ,  $\omega$ : angular frequency,  $c_0$ : speed of light in vacuum,  $n$ : refractive index of medium). Thus, optical accesses, for instance in Raman and THz spectroscopy, to the magnetic transitions are focused on the zone-center magnons.<sup>[3–8]</sup> On the other hand, neutron scattering covers a broad range in the Brillouin zone due to large momenta of neutrons, promoting this technique as ideal spectroscopic tool to map spin-wave dispersion. In reality, however, the picture is tainted by the low energy and wavevector resolution of neutron scattering experiments and restriction to large-scale facilities. Further constraints arise from the required large sample mass and the preference to avoid hydrogen and other isotopes with strong neutron absorption. In turn, optical techniques could provide easy access to the magnetism albeit the  $q \approx 0$  constraint. Attempts to overcome this constraint are subject of current research and first promising results have been reported.<sup>[9–11]</sup>

In THz spectroscopy, with the aid of ultrafast lasers and advanced detection schemes, dynamical processes in the (sub-)picosecond range become accessible.<sup>[12,13]</sup> This progress allows not only performing time-resolved studies but enables a control of magnetization dynamics.<sup>[14–16]</sup> Magnetic properties can be probed, for instance, through the magneto-optical Faraday or Kerr effects.<sup>[17,18]</sup> Other examples include the coherent generation of magnons.<sup>[11]</sup> Control over THz-driven spin precession<sup>[19–22]</sup> opens the field of THz magnetometry, that is, the fully optical extraction of magnetic properties.<sup>[23]</sup>

Here, we demonstrate the potential of THz time-domain spectroscopy (THz-TDS)<sup>[24]</sup> in easing its zone-center restriction: the spin (magnon) density of states (SDOS) can be probed over the entire Brillouin zone via multi-center magnon absorption in materials with several magnetic sublattices. In this picture, magnon excitations take place simultaneously in different magnetic sublattices and positions in momentum space,  $q_n$ .<sup>[25–27]</sup> Yet, the summed momenta of the participating magnons are zero,  $\sum_n q_n \approx 0$ , achieving momentum conservation. **Figure 1a** compares the conventional excitation picture, that is, one-magnon process ( $q \approx 0$ ), with the multi-center magnon process ( $\Delta q \approx 0$ ). The distinction between both is prominent in the THz susceptibility  $\chi''_m$  and in the time-dependent electric field of the probing light. Here, the  $q \approx 0$  mode (one-magnon) causes a homogeneous precession of spins,<sup>[14,28]</sup> resulting in sharp spectral features in  $\chi''_m$  and relatively long oscillations of the electric field (20–40 ps)<sup>[29,30]</sup> through a free induction decay mechanism.<sup>[19–22]</sup> The multi-center magnon absorption yields a broad feature<sup>[25,31,32]</sup> implying a reduced lifetime (cf. red and yellow contributions in Figure 1a). It can be observed even above the magnetic long-range ordering temperature  $T_N$  as a semblance of paramagnons (paramagnons are observed by various methods, see refs. [33–35]).

We have chosen the quantum magnet<sup>[36–40]</sup> Y-kapellasite ( $Y_3Cu_9(OH)_{19}Cl_8$ )<sup>[41]</sup> as our material platform. Y-kapellasite forms a distorted kagome lattice and has attracted attention recently due to its intriguing magnetic ground state ( $T_N = 2.2$  K), suggested in Figure 1b<sup>[42]</sup>. Here, the magnetic supercell is comprised of three hexagons rotated by  $120^\circ$ . Due to the three possible arrangements, we define each hexagon as a magnetic

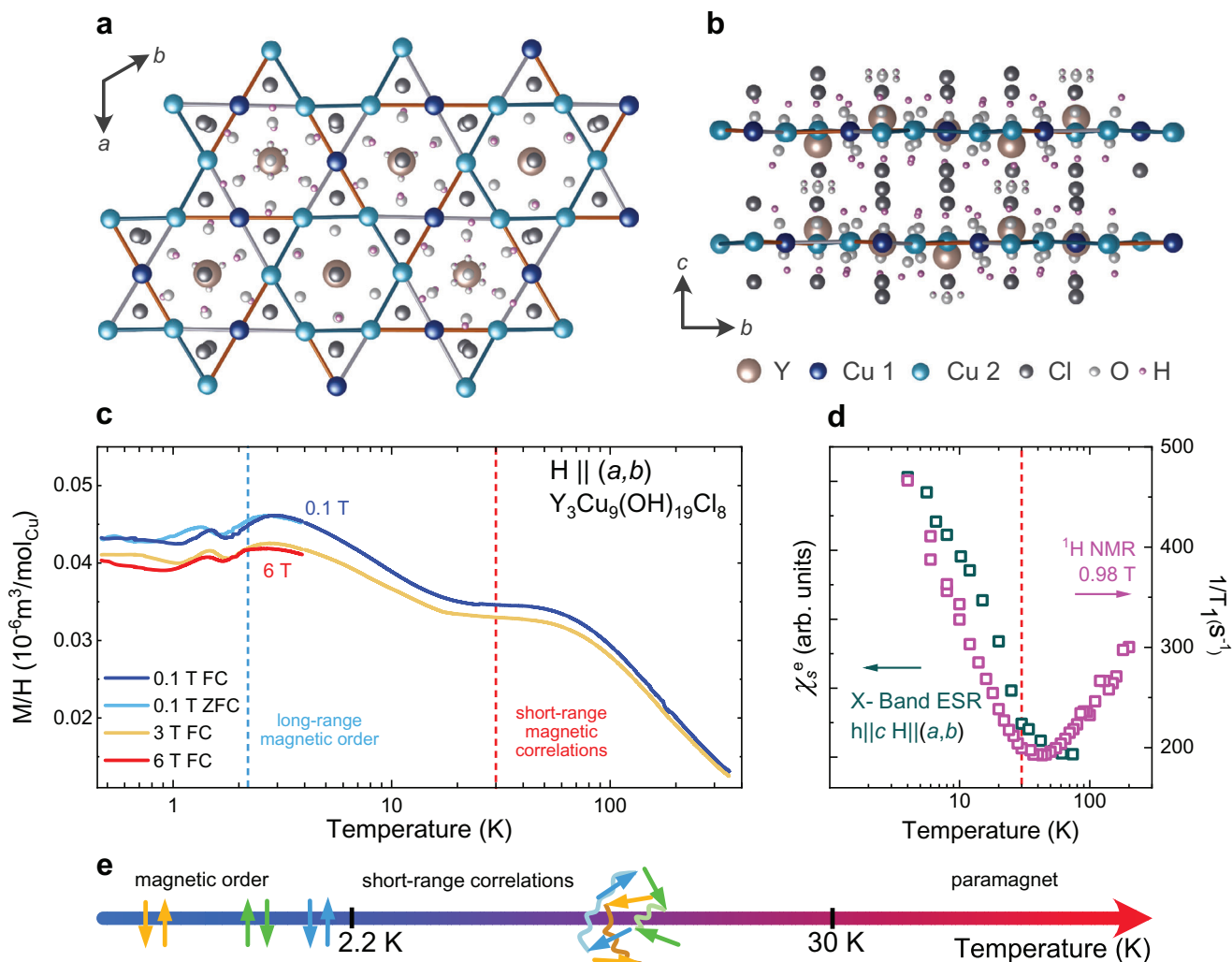


**Figure 2.** Crystal structure and magnetic properties of Y-kapellasite. a) In-plane, ( $a, b$ )-direction and b) out-of-plane ( $c$ -axis) crystal structure. Different copper sites, including the distorted kagome bonds (blue, red, gray) are depicted in cyan and dark blue. c) Temperature-dependent dc magnetic susceptibility  $M/H$  (FC - field cooled, ZFC - zero field cooled), under several in-plane magnetic fields. The red dashed line correspond to the onset of short-range magnetic correlations, the light blue dashed line indicates the onset of long-range magnetic order. d) Spin-lattice relaxation rate  $1/T_1$  ( $^1\text{H}$  NMR, right axis) and electron spin susceptibility  $\chi_s^e$  (ESR, left axis). Red dashed line: Onset of short-range magnetic correlations. e) Extracted temperature ranges, onset of short-range magnetic correlations (30 K) and long-range magnetic order (below 2.2 K).

sublattice and give it one of the colors: green, blue, or yellow. Strong short-range magnetic correlations and persistent spin dynamics below the ordering temperature (down to  $T = 20$  mK) were reported previously.<sup>[41,43]</sup> The THz transmission of Y-kapellasite was measured over a wide temperature and magnetic field range. At low temperatures ( $T < 30$  K), we find magnetically active, continuum-like excitations decaying through oscillations of the transient electric field during an extended time period of around 5 ps. By comparison to the linear spin-wave theory (LSWT), we conclude that the THz  $\chi_m''$  encodes the SDOS through a multi-center magnon absorption, three-center magnon, augmented by the distinct magnetic ground state of Y-kapellasite, as described in Figure 1b. We propose THz magnetometry via multi-center magnon absorption as a method to overcome the conventional zone-center restriction providing access to magnetism over the entire Brillouin zone.

## 2. Results

### 2.1. Magnetic Properties of Y-Kapellasite

In Y-kapellasite, a distorted kagome lattice is formed by two distinct Cu sites, as depicted in Figure 2a. Here, the magnetic superexchange is governed along three different Cu–O–Cu paths.<sup>[41,42]</sup> The distorted kagome planes stack along the  $c$ -direction (Figure 2b). See Supporting Information for further material information (Figures S1 and S2, Supporting Information). Let us first consider the static response of the spin system. The in-plane magnetic susceptibility ( $H \parallel (a, b)$ ) down to temperatures as low as  $T = 400$  mK is presented in Figure 2c. Focusing on the  $H = 0.1$  T measurements, upon cooling, the magnetization first saturates in a plateau at intermediate temperatures ( $T = 50$  K) and continues to rise below  $T = 30$  K. At around

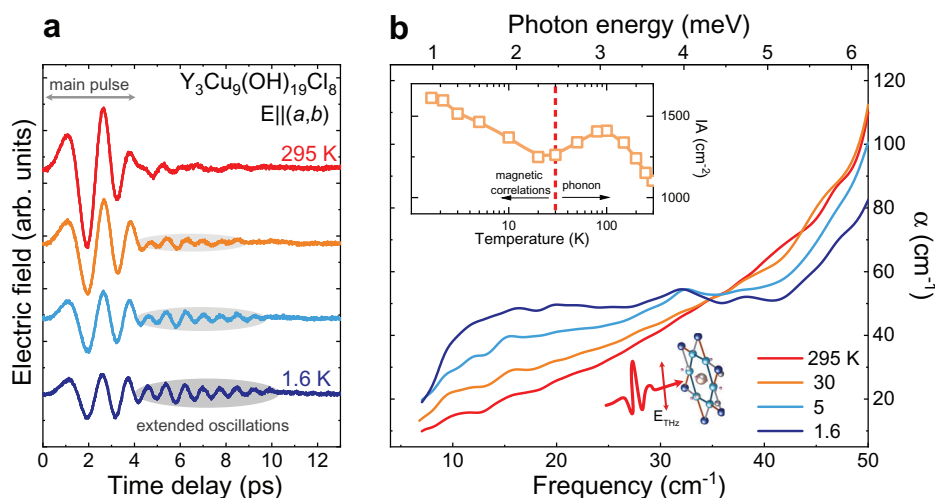


**Figure 3.** Temperature-dependent THz spectra. a) THz electric field, transmitted through Y-kapellasite as a function of time delay and b) resulting absorption coefficient  $\alpha$  for the in-plane direction, as depicted ( $E_{\text{THz}} \parallel (a, b)$ ). At  $T = 295$  K, the main pulse (0 to 4 ps) contains most of the THz responses (phononic properties). Below the onset of short-range magnetic correlations,  $T = 30$  K, the THz electric field pronounces extended-time oscillations (4 to 10 ps, shaded area), while the main pulse loses its intensity. As a result the continuum-like absorption develops in  $\alpha$ , followed by two additional peak-like features at  $32$  and  $37$   $\text{cm}^{-1}$ . Inset: Integrated absorption coefficient IA (up to  $40$   $\text{cm}^{-2}$ ). The red dashed line represent the onset of short-range magnetic correlations,  $T = 30$  K. Above  $T = 30$  K, changes in IA are mostly caused by the lowest in-plane phonon mode. Below the onset of short-range magnetic correlations, the IA continuously increases.

$T = 3$  K a maximum develops, followed by a smaller peak at lower temperature ( $T = 1.5$  K). While the maximum at  $T = 3$  K is consistent with the previously reported  $T_N = 2.2$  K,<sup>[41]</sup> also observed in heat-capacity measurements, the additional smaller peak suggests a successive freezing of the magnetic texture at lower temperatures. This is in accordance with the recent muon spin relaxation study on polycrystalline samples,<sup>[43]</sup> reporting persistent spin dynamics down to the mK range. Furthermore, a weak hysteresis between field cooled (FC) and zero field cooled (ZFC) measurements is observed below  $T = 3$  K, whereas the cooling protocol does not affect the susceptibility noticeably at higher temperatures, indicating the contribution of uncompensated spins at low temperatures. Increasing the external magnetic field, the magnetization is slightly suppressed and the 3 K-peak shifts to lower temperatures, implying dominant antiferromagnetic interactions. This result suggests two different characteristic temperatures in Y-kapellasite, around  $T = 30$  K and  $T_N = 2.2$  K.

For additional information, the magnetic properties of Y-kapellasite are further investigated using nuclear magnetic resonance (NMR) and electron spin resonance (ESR). Starting with the  $^1\text{H}$ -NMR characterization (Figure 2d), the in-plane spin-lattice relaxation rate  $1/T_1$  first decreases upon cooling and increases again near  $T = 30$  K. This crossover indicates the onset of short-range magnetic correlations. A similar temperature scale is found by ESR measurements as shown in Figure 2d, left axis (Figure S3, Supporting Information for extended ESR spectra). Simultaneously with the onset of magnetic correlations at around  $T = 30$  K, the electron spin susceptibility  $\chi_s^e$  starts to rise, advocating the close relation between the ESR absorption and the short-range magnetic interactions. Additional measurements, high-field magnetization and ac susceptibility, reveal similar temperature scales and are presented in the Supporting Information (cf. Figures S4 and S5, Supporting Information). The range between  $T \approx 30$  K (short-

range magnetic correlations) and  $T_N \approx 2.2$  K offers experimental access for investigating the emergence of magnetism on the kagome lattice above  $T_N$ , as sketched in Figure 2e. The desired multi-center magnon absorption could survive for higher temperatures through these short-range magnetic correlations.

## 2.2. THz Time-Domain Spectra as a Probe of Spin Dynamics

In Figure 3 we plot the raw data of the THz-TDS recorded in the  $ab$ -plane. At high temperatures, the in-plane time-domain signal of the transient electric field (Figure 3a) consists of only the main pulse ranging from 0 to 4 ps (see Section 5). With cooling, the intensity of this pulse decreases, but in addition a prolonged oscillating electric field develops over an extended time ranging from 4 to 10 ps. Note, for conventional one-magnon excitations, a similar time-domain signal was reported but on a significantly longer time scale (several tens of ps).<sup>[20–22,29,30]</sup> To gain more insight into the underlying physical processes, we perform a Fourier transformation and calculate the frequency-dependent absorption coefficient  $\alpha$ , plotted in Figure 3b. At room temperature, only the tail of the lowest in-plane phonon mode contributes notably to the THz absorption. Upon cooling, the phonon contribution first increases slightly and then becomes weaker together with a suppression of the main pulse in the time-domain signal (see Figure S6, Supporting Information, for the results of infrared spectroscopy and density functional theory [DFT] calculations of the phonons). As the temperature drops below  $T = 30$  K, we see the low-frequency absorption rising, resulting in a broad continuum-like contribution much stronger than the phonon (in this frequency range). This corresponds to the enhancement of the electric field oscillations at extended times as illustrated in Figure 3a. The feature increases strongly with further cooling and finally

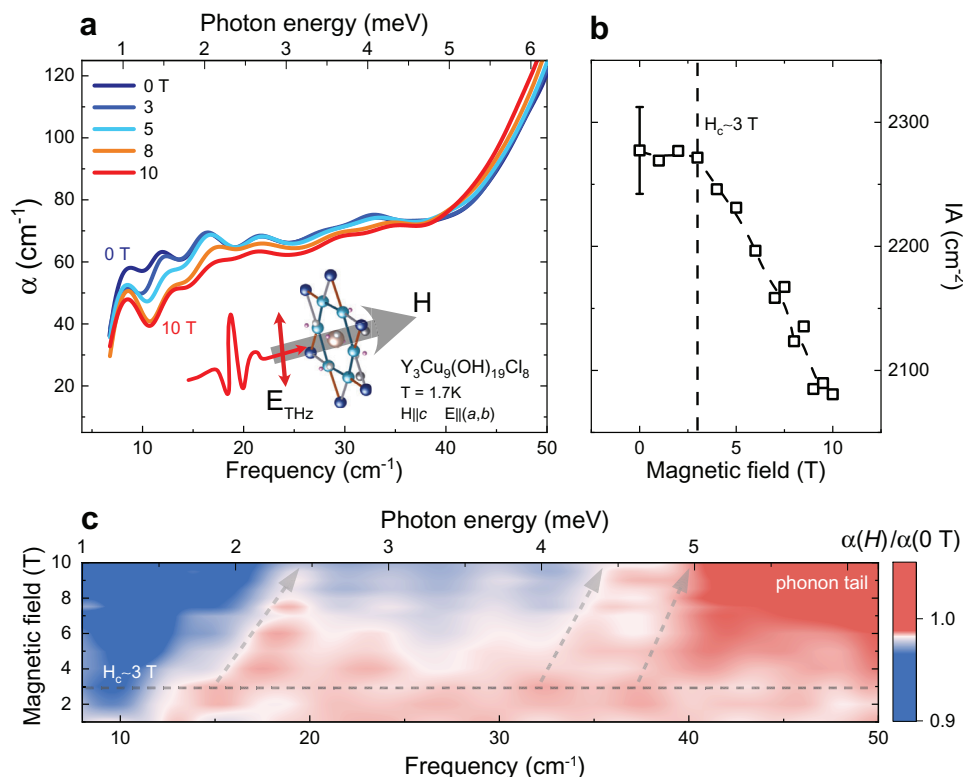


**Figure 4.** Result of magneto-THz spectroscopy at 1.7 K. a) Absorption coefficient  $\alpha$  under magnetic field in Faraday geometry, as depicted ( $H \parallel c$ ,  $E_{\text{THz}} \parallel (a, b)$ ). The THz continuum-like absorption decreases with increasing magnetic fields, confirming its magnetic origin. b) Integrated absorption coefficient IA (up to  $40 \text{ cm}^{-1}$ ), exposing a critical magnetic field of  $H_c \approx 3 \text{ T}$ . c) Contour plot of the relative absorption coefficient under magnetic field  $\alpha(H)/\alpha(0 \text{ T})$ , normalized to zero field. The gray arrows indicate the field evolution of the onset of the continuum-like absorption and of the two peak-like features at  $32$  and  $37 \text{ cm}^{-1}$ .

dominates the entire THz response down to the lowest temperature measured. Furthermore, for  $T < 5 \text{ K}$ , we observe two weaker, but noticeable, peak-like contributions between  $30 - 40 \text{ cm}^{-1}$ . Despite the increase of intensity, no qualitative difference can be found in measurements below  $T_N$ . From the comparison with our calculations, we can exclude a phononic origin of the low-energy features. Also electronic contributions are unlikely for the highly insulating Y-kapellasite (bandgap of  $3.6 \text{ eV}$ ).<sup>[41,44]</sup>

These trends become even more obvious when looking at the integrated absorption IA (similar to the spectral weight, see Section 5), displayed in the inset of Figure 3b. The crossover range in  $IA(T)$  matches well with the onset of short-range magnetic correlations at around  $T = 30 \text{ K}$  as observed in the NMR spin-lattice relaxation rate and ESR susceptibility. This good agreement between the temperature scales strongly suggests that the THz continuum-like absorption is caused by short-range magnetic correlations even above  $T_N$  (see Figure S7, Supporting Information for corresponding spectra covering the entire temperature range; Figure S8, Supporting Information for additional data in the frequency domain).

### 2.3. Magneto-THz Spectroscopy

To clarify the magnetic origin of this continuum-like absorption, we carried out magneto-THz measurements at  $T = 1.7 \text{ K}$  while

applying a static magnetic field up to  $H = 10 \text{ T}$  in Faraday geometry. With ramping up the magnetic field, the continuum-like feature loses its intensity beginning at the low-frequency end, as displayed in Figure 4a (Figure S9, Supporting Information for extended data). This can be nicely seen in Figure 4b where the IA is plotted as a function of  $H$ . Exceeding a critical field of  $H_c = 3 \text{ T}$ ,  $IA(H)$  decreases considerably; at a field strength of  $H = 10 \text{ T}$  the intensity is reduced by almost 10%. This quantitative change seems reasonable since the magnetic energy corresponds to roughly 10% of the exchange energy:  $\mu_B H = 0.1 k_B \Theta_{\text{CW}} \approx 0.1 J$ , where  $\Theta_{\text{CW}} \approx -100 \text{ K}$  is the Curie-Weiss temperature and  $J \approx 13 \text{ meV}$  is the dominating exchange energy ( $\mu_B$  is Bohr magneton,  $k_B$  is Boltzmann constant).<sup>[41,42]</sup> The phonon tail above  $40 \text{ cm}^{-1}$  is affected as well: it weakly shifts toward lower energies. In addition to these obvious changes in the spectrum, we can identify some more subtle variations inside the continuum-like absorption. Slight shifts of the  $30 - 40 \text{ cm}^{-1}$  peaks become clearer in the contour plot of the normalized absorption coefficient  $\alpha(H)/\alpha(0 \text{ T})$ , presented in Figure 4c. Interestingly, the onset of the continuum-like absorption shows a stronger change under magnetic field, compared to the  $30 - 40 \text{ cm}^{-1}$  peaks, cf. gray arrows in Figure 4c. Note the reduced signal-to-noise ratio of a magneto-optical measurement leads to somewhat noisy features below  $20 \text{ cm}^{-1}$ ; nevertheless, our magneto-optical THz results strongly support the magnetic origin of the continuum-like feature.



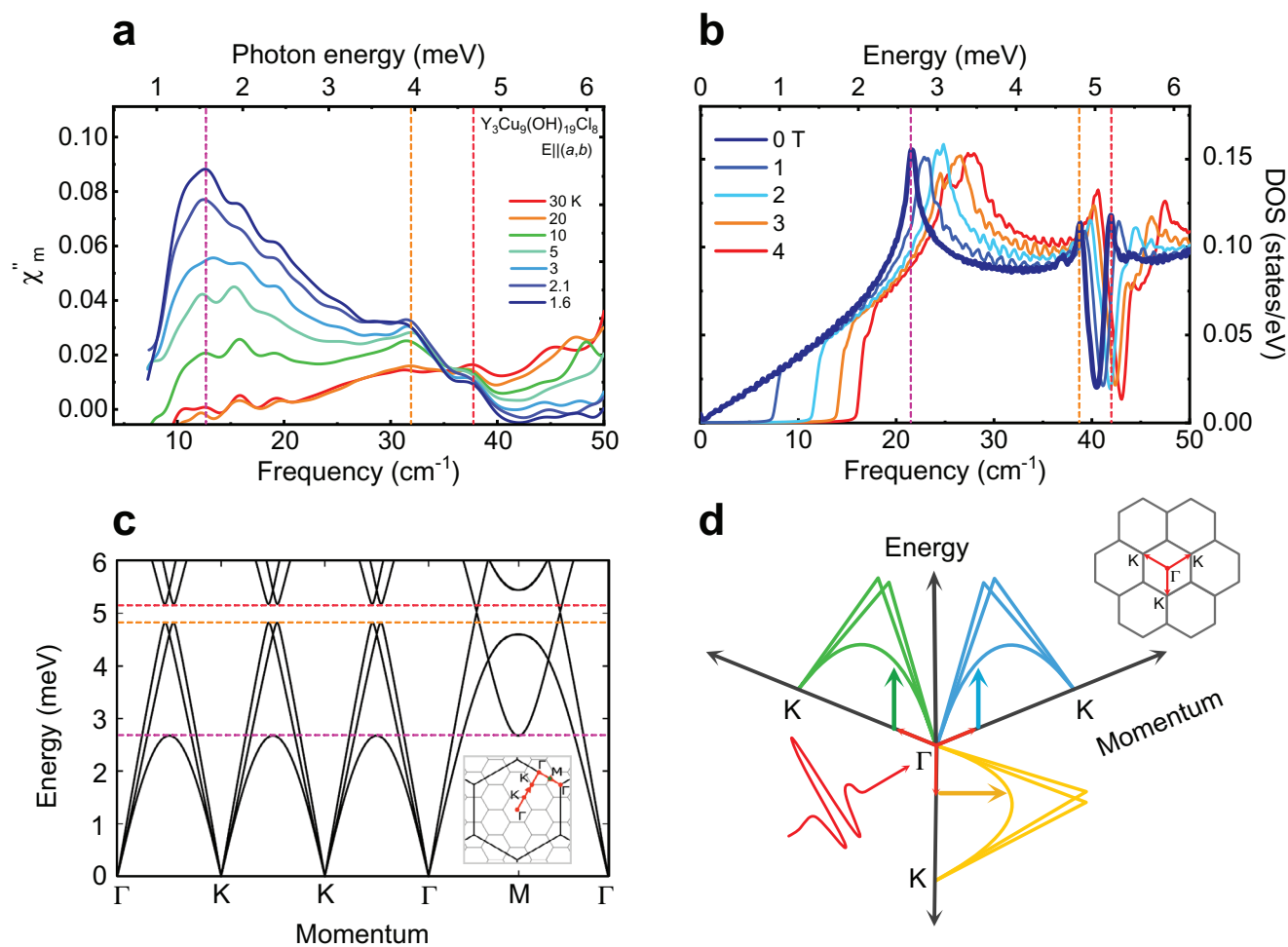


**Figure 5.** Three-center magnon excitations and theoretical spin-wave dispersion of Y-kapellasite. a) The frequency-dependent imaginary part of the magnetic susceptibility  $\chi''_m$  obtained from THz-TDS exposes the natural spectral form of the three-center magnon excitations. Three distinctive features are marked by vertical dashed lines. b) SDOS obtained from LSWT calculations with and without magnetic field. The SDOS shows three characteristic energies below 6 meV with a high density of states (vertical dashed lines). c) Spin-wave dispersion of Y-kapellasite. Horizontal dashed lines: Corresponding to the energies in (b). Inset: Calculated path in the extended Brillouin zone (black hexagon). d) The three-center magnon process in momentum space, that is, three spin excitations in the different magnetic sublattices (green, blue, and yellow color code) with  $0 \approx \sum_n \mathbf{q}_n$ .

## 2.4. Multi-Center Magnon Excitations

In a next step we have to separate the magnetic contributions from the dielectric ones in the THz absorption in order to reveal their natural spectral form. With the fair assumption that the dielectric properties do not change drastically at low temperatures, the magnetic susceptibility  $\chi''_m$  can be obtained from the THz spectra (Figure 3) by referencing to the 80 K-spectrum (see Section 5 for further information). The results are shown in **Figure 5a**. The extraction of  $\chi''_m$  unveils an asymmetric shape of the magnetic continuum-like feature with a maximum at around  $12 \text{ cm}^{-1}$  and a width of about  $30 \text{ cm}^{-1}$  followed by two peaks at  $32$  and  $37 \text{ cm}^{-1}$  at the lowest temperature,  $T = 1.6 \text{ K}$ .

To learn more about the origin of the magnetic THz response and the magnetic ground state, we calculated the spin-wave dispersion for Y-kapellasite with LSWT by assuming a coplanar non-collinear  $\mathbf{Q} = (1/3, 1/3)$  magnetically ordered ground state as suggested by recent ab initio DFT calculations.<sup>[42]</sup>

This ordered state comprises three different magnetic sublattices of hexagons (shown as green, blue, and yellow in Figure 1b). Within each hexagon, the spins are antiferromagnetically coupled and neighboring hexagons are coupled to each other via spins (shown in gray) whose directions are fully determined by the neighboring hexagons (slave spins).<sup>[42]</sup>

Figure 5b,c contain the calculated SDOS and the corresponding spin-wave dispersion in the relevant energy range, below 6 meV (1 meV corresponds to  $8.065 \text{ cm}^{-1}$ ). Several energies with a density of states, corresponding to characteristic energy scales of the THz  $\chi''_m$ , are marked by dashed lines. The spin-wave dispersion of Y-kapellasite is gapless and degenerated at the  $\Gamma$ -point (Goldstone mode); possible one-magnon excitations are outside our THz spectral range (Figure S10, Supporting Information). As introduced above, a one-magnon process only measures the response at the zone center; in stark contrast to multi-center magnon excitations that can expand over the entire Brillouin zone. For the latter

case, due to momentum conservation, the total wavevector of the participating magnons must be zero,  $\sum_n \mathbf{q}_n \approx 0$ , which is accomplished by the simultaneous magnon excitations in three distinct magnetic sublattices. Within this picture, the steady development of the continuum-like absorption without any additional features across  $T_N$  can be explained by multi-center magnon absorptions. The one-magnon excitations are outside our accessible spectral range and only the multi-center magnons are observed. As illustrated in Figure 5d, the spin-wave dispersion beyond the  $\Gamma$ -point gets accessible via such excitations. Indeed, toward the K-direction the degeneracy is lifted and the lowest band exhibits a parabolic shape (Figure 5c). Around 2.7 meV the band flattens and reaches a maximum. This shape of the dispersion yields a large number of available states in the low-energy range and generates the maximum in the SDOS at 2.7 meV which is related to the peak at 1.5 meV ( $12 \text{ cm}^{-1}$ ) in  $\chi''_m$ . At higher energies, around 4.8 meV, the SDOS increases again with the next two higher-lying bands reaching their maxima. At 5 meV the number of available states drops significantly before it peaks again at around 5.2 meV (parabola minima of the next higher bands). Indeed, these states are related to the peak-like contributions between  $32$  and  $37 \text{ cm}^{-1}$  (4 and 4.6 meV) in  $\chi''_m$  (Figure 5a). There is a small offset of about 1 meV between experimental results and calculations, probably due to a small mismatch in parameters between experiment and theory.

Overall, including the multi-center magnon picture, the SDOS from the LSWT calculations shows a remarkable agreement with the experimental result,  $\chi''_m$ . Furthermore, based on the SDOS, we calculated the expected  $\chi''_m$ , validating the observed spectral shape (cf. Figure S11, Supporting Information). The agreement with theory even extends to the magnetic field dependence. Figure 5b displays the change of the SDOS with magnetic field. Under external magnetic field, the spin-wave dispersion becomes gapped and the weight of the SDOS shifts up in energy (Figures S12 and S13, Supporting Information). In addition, the 2.7 meV maximum reveals a strong shift under magnetic field, it is slightly different than the one obtained for the 4.8 and 5.2 meV peaks. We note that the calculations overestimate the magnetic field scale compared to that of the experiment, perhaps due to demagnetization effects. Still, these trends under external magnetic field are corroborating the result of our magneto-THz spectroscopy, displayed in Figure 4.

### 3. Discussion

Our THz study allows to directly probe the SDOS via optical spectroscopy; by utilizing multi-center magnon absorption we gain access to the SDOS over the entire Brillouin zone, that is, we actually perform THz magnetometry. In Y-kapellasite, strong short-range magnetic correlations lead to spin fluctuations over a wide temperature range. The paramagnonic behavior is aided by these fluctuations explaining the development of the THz continuum-like absorption together with the onset of short-range magnetic correlations. The lattice distortion, on the other hand, lowers the spatial symmetry and generates three magnetic sublattices. This distortion is decisive for multi-center magnon excitations to occur. In particular, the magnetic superstructure favors simultaneous  $3N$  magnon excitations where each of the participating magnon excitations occurs, respectively, at one of the three

magnetic sublattices, that is three-center magnon, while in total the net momentum is conserved ( $\Delta \mathbf{q} = \mathbf{q}_{ph} \approx 0$ ), as illustrated in Figure 1b (see Supporting Information for further discussion, Figure S14, Supporting Information). We suggest that the role of distortion could be further verified in other kagome lattices.<sup>[42,45–47]</sup> But for the case of Y-kapellasite, the distortion seems to be crucial for the multi-center magnon absorption given that Herbertsmithite, which is considered as a perfect kagome structure,<sup>[39]</sup> does not reveal any signature of multi-center magnons (Figure S15, Supporting Information).<sup>[48,49]</sup>

Such a symmetry breaking can also be phonon-assisted.<sup>[50,51]</sup> We note that similar suggestions were made for the parent compound of cuprates with an underlying square lattice. In those cases, the observed features were associated with the coupling between magnons and phonons leading to enhanced excitation frequencies in the mid-infrared range.<sup>[52,53]</sup> The magneto-elastic coupling may be represented in the temperature dependence of the phonon modes. In the present case, we observe unusual redshifts and anomalies of the infrared-active phonons accompanied by the development of short-range magnetic correlations (Figure S6, Supporting Information).

Overall, the comparison of our experimental results with LSWT calculations suggests that for a proper description a multi-center magnon picture is required: we have to go beyond a simple magnetic mode in order to explain the THz excitations. In fact, the multi-center magnon absorption in Y-kapellasite resembles the conventional two-center magnon absorption observed in classical antiferromagnets:  $\text{FeF}_2$ ,  $\text{MnF}_2$ ,  $\text{CoF}_2$ , and  $\text{NiF}_2$ .<sup>[25,27,31,54–57]</sup> Utilizing Dexter's theory of cooperative optical absorption,<sup>[58]</sup> earlier reports proposed several mechanisms,<sup>[54,55,59]</sup> where the removal of centrosymmetric points is supposed to be particularly necessary for the non-vanishing electric dipole moment.<sup>[27]</sup>

The former studies confined the two-center magnon absorption as electric dipole active phenomena; but there is no reason for this limitation. Recently, a direct coupling between the magnetic state and light was proposed; the detection takes place over the free induction decay.<sup>[19–22]</sup> As well, accounting for the two magnetic sublattices in conventional antiferromagnets, traditionally only a two-center absorption was considered. Moreover, the optical selection rule for the three-center magnon excitation might differ from the conventional one-magnon picture ( $\Delta S = \pm 1$ , the spin difference between initial and excited state). For example, the two-center magnon excitation was discussed before with an altered optical selection rule.<sup>[60,61]</sup> All these now turn into limiting factors when a more detailed and generalized microscopic picture has to be established for the multi-center magnon absorption. Together with a refined understanding, our approach might be applicable in a large pool of materials.

We further discuss the relation of the THz multi-center magnon absorption to similar multimagnon processes observed in other quantum magnets of low symmetry. For quantum magnets, often a virtual process via the magnon decay<sup>[62]</sup> is discussed, which has been observed in Raman / neutron scattering.<sup>[63–66]</sup> Note that multimagnon scattering (photon / neutron scatters by creating multiple magnons) and THz multi-center magnon absorption (multi-center magnon: one photon gets absorbed, simultaneously creating multiple magnons in different magnetic sublattices) need to be discerned with distinct optical selection rules.<sup>[27]</sup> Moreover, the higher-order

magnon contributions beyond LSWT are as well discussed in THz absorption.<sup>[67]</sup> However, these are different from the multi-center magnon absorption, subject of our study. Regarding higher-order magnons, mixing of one-magnon branches with multimagnon states can occur as a result of the low symmetry of the spin interactions as in  $\alpha$ -RuCl<sub>3</sub>.<sup>[68,69]</sup> A further example can be found in the case of Yb<sub>2</sub>Ti<sub>2</sub>O<sub>7</sub>, showing a field-induced decay of the one-magnon branch into a two-magnon continuum.<sup>[63]</sup> In Y-kapellasite, however, neither geometrical frustration nor anisotropic spin interactions seem to be present in the system<sup>[42]</sup> excluding the magnon decay processes from the present case. Nevertheless, we note that a multi-center magnon based extraction of the SDOS with THz spectroscopy, as presented in this work, might be possible even in the presence of a decay mechanism.

There are several issues concerning the magnetic properties of Y-kapellasite which should be addressed in future investigations. One particularly interesting issue remaining is the persistent spin dynamics in the magnetically ordered state below  $T_N = 2.2$  K<sup>[43]</sup> which might be related to the successive spin freezing observed in the susceptibility, Figure 2c. For optical measurements, such a low temperature (mK range) is still challenging. Hence, complementary experimental techniques are required to scrutinize this exotic behavior. In addition, an investigation of the microscopic origin of the short-range magnetic correlations much above  $T_N$  could be a focus of further studies.

## 4. Conclusion

In conclusion, in our proof-of-principle experiment, we establish THz-TDS as a method to directly probe the SDOS expanding its capability from  $q \approx 0$  to  $\Delta q \approx 0$  excitations over the entire Brillouin zone: THz magnetometry. The three-center magnon absorption in the exotic magnetic superstructure of Y-kapellasite is the key mechanism behind this observation. Driven by short-range magnetic interactions, the absorption persists well above the magnetic ordering temperature, that is, we do observe paramagnons. The multi-center magnon absorption allows easy access to the SDOS for suitable magnets, in particular in systems with low symmetry.

## 5. Experimental Section

**Crystal Growth and Characterization:** Crystals were grown via a horizontal external gradient growth method. This optimized synthesis led to nearly perfect defect-free single crystals with large facets (kagome-planes between 2 and 3 mm and thickness of around 0.5–1 mm), see Figure S1, Supporting Information. The results of X-ray diffraction is presented in Figure S2, Supporting Information. The ac and dc magnetic susceptibilities were measured as explained in the Supporting Information.

**THz-TDS Measurements:** THz-TDS measured the time-dependent electric field.<sup>[24]</sup> Through a fast Fourier transformation (FFT), intensity and phase could be obtained. This allowed to directly calculate the optical response functions.<sup>[1,2]</sup> A typical time-trace of the transient electric field showed an oscillating behavior with a strong pulse at early times (main pulse). Due to their short lifetime, electronic transitions or phononic resonances were, in general, contained in the main pulse. However, phenomena with a longer lifetime, such as magnetic resonances, could extend to longer times (over several tens of ps), exceeding the main pulse.<sup>[20–22,29,30]</sup>

THz-TDS measurements were carried out in transmission geometry on oriented single crystals ( $E_{\text{THz}} \parallel (a, b)$ ) at several temperatures between

295 and 1.6 K with a helium bath cryostat. Magneto-optical THz measurements were performed in Faraday geometry ( $E_{\text{THz}} \parallel (a, b)$ ,  $H \parallel c$ ) with static magnetic field strengths up to  $H = 10$  T and temperatures down to 1.7 K. The absorption coefficient  $\alpha$  was calculated from the transmittance  $\text{Tr}$  by  $\alpha = -\ln\{\text{Tr}\}/d$ , where  $d$  is the sample thickness. The integrated absorption coefficient  $IA = \int \alpha d\omega$  resembled the optical spectral weight and provided a quantitative access to the spectral features (see Supporting Information for further information). The frequency-dependent magnetic susceptibility  $\chi_m'' = \text{Im}\{\tilde{\chi}_m(\omega)\}$  was calculated by referencing to the high-temperature dielectric response,<sup>[5,7,8,70]</sup> that is, the  $T = 80$  K spectrum, see Supporting Information for further information. This quantity encoded the SDOS, as previously shown for the  $q \approx 0$  case.<sup>[5]</sup>

**ESR Measurements:** Temperature-dependent ESR measurements in the X-band frequency were carried out. The in-plane response was determined with a microwave field  $h \parallel c$  and external magnetic field  $H \parallel (a, b)$ . More details are discussed in the Supporting Information.

**NMR Characterization:** <sup>1</sup>H-NMR experiments were performed on a  $3 \times 3 \times 1$  mm<sup>3</sup> sized Y-kapellasite single crystal with magnetic field ( $H = 0.98$  T) aligned parallel to the kagome layers ( $H \parallel (a, b)$ ). The spin-lattice relaxation rate  $1/T_1$  was measured by non-selective excitation of the full line.  $1/T_1$  was determined through saturation-recovery using single-exponential fits. Temperature control in the range from 4 to 200 K was achieved using a <sup>4</sup>He cryostat with a variable-temperature insert.

**High-Field Magnetization:** The high-field magnetization was determined between  $T = 0.5$  and 30 K in pulsed magnetic fields up to 55 T for in-plane and out-of-plane orientations. Further information can be found in the Supporting Information. Measurements were performed at the high field laboratory in Dresden, Germany (HLD-EMFL).

**DFT and LSWT Calculations:** The phonon frequencies were calculated using a combination of the PHONOPY package<sup>[71,72]</sup> and DFT as implemented in the Vienna ab Initio Simulation Package code.<sup>[73–75]</sup> The details of the calculations are in the Supporting Information. The magnon dispersion was determined by using LSWT as implemented in SpinW 3.0.<sup>[76]</sup> The details are explained in the Supporting Information.

## Supporting Information

Supporting Information is available from the Wiley Online Library or from the author.

## Acknowledgements

The authors thank Artem Pronin, Guratinder Kaur, and Reinhard K. Kremer for fruitful discussion, Björn Miksch and Lena N. Majer for help with the ESR measurements and Gabriele Untereiner for continuous technical support. The project was supported by the HLD-HZDR, member of the European Magnetic Field Laboratory (EMFL), and the Deutsche Forschungsgemeinschaft (DFG). A.R. and R.V. thank the DFG through TRR 288-422213477 (project A05). Y.L. acknowledges support by China Postdoctoral Science Foundation (Grant No. 2019M660249) and National Natural Science Foundation of China (Grant No. 12004296). M.M. acknowledges the Swiss National Science Foundation (Grant No. 206021\_139082). A.P. acknowledges support by the Alexander von Humboldt Foundation through the Feodor Lynen Fellowship. The work at University of California, Los Angeles, was supported by NSF Grant 2004553.

Open access funding enabled and organized by Projekt DEAL.

## Conflict of Interest

The authors declare no conflict of interest.

## Author Contributions

T.B. and S.R. contributed equally to this work. T.B. and S.R. performed the spectroscopic measurements and analyzed the data. P.P., K.M.Z., and C.K.



grew the crystals. P.P., J.W., S.S., D.G., Y.S., and M.M. performed the magnetic characterization. J.N. performed the structural characterization. A.P. and S.E.B did the NMR measurements. A.R. performed the LSWT analysis. Y.L. calculated the phonon dispersion. A.P. contributed to the infrared measurements. T.B., S.R., and P.P. wrote the manuscript with input from all authors. P.P., T.B., and S.R. initiated the project. M.D. and R.V. supervised the project.

## Data Availability Statement

The data that support the findings of this study are available from the corresponding author upon reasonable request.

## Keywords

kagome lattices, multi-center magnons, terahertz magnetometry, terahertz photons

Received: March 4, 2022

Published online: March 25, 2022

- [1] M. Dressel, G. Grüner, *Electrodynamics of Solids: Optical Properties of Electrons in Matter*, Cambridge University Press, Cambridge **2002**.
- [2] D. B. Tanner, *Optical Effects in Solids*, Cambridge University Press, Cambridge **2019**.
- [3] R. S. Fishman, J. A. Fernandez-Baca, T. Rööm, *Spin-Wave Theory and its Applications to Neutron Scattering and THz Spectroscopy*, Morgan & Claypool Publishers, San Rafael **2018**.
- [4] D. Wulferding, Y. Choi, W. Lee, K.-Y. Choi, *J. Condens. Matter Phys.* **2019**, 32, 043001.
- [5] X. Zhang, F. Mahmood, M. Daum, Z. Dun, J. A. M. Paddison, N. J. Laurita, T. Hong, H. Zhou, N. P. Armitage, M. Mourigal, *Phys. Rev. X* **2018**, 8, 031001.
- [6] A. Little, L. Wu, P. Lampen-Kelley, A. Banerjee, S. Patankar, D. Rees, C. A. Bridges, J.-Q. Yan, D. Mandrus, S. E. Nagler, J. Orenstein, *Phys. Rev. Lett.* **2017**, 119, 227201.
- [7] P. Chauhan, F. Mahmood, H. J. Changlani, S. M. Koohpayeh, N. P. Armitage, *Phys. Rev. Lett.* **2020**, 124, 037203.
- [8] N. J. Laurita, J. Deisenhofer, L. Pan, C. M. Morris, M. Schmidt, M. Johnsson, V. Tsurkan, A. Loidl, N. P. Armitage, *Phys. Rev. Lett.* **2015**, 114, 207201.
- [9] T. M. H. Nguyen, L. J. Sandilands, C. H. Sohn, C. H. Kim, A. L. Wysocki, I.-S. Yang, S. J. Moon, J.-H. Ko, J. Yamaura, Z. Hiroi, T. W. Noh, *Nat. Commun.* **2017**, 8, 251.
- [10] L. Wu, A. Little, E. E. Aldape, D. Rees, E. Thewalt, P. Lampen-Kelley, A. Banerjee, C. A. Bridges, J.-Q. Yan, D. Boone, S. Patankar, D. Goldhaber-Gordon, D. Mandrus, S. E. Nagler, E. Altman, J. Orenstein, *Phys. Rev. B* **2018**, 98, 094425.
- [11] J. R. Hortensius, D. Afanasiev, M. Matthiesen, R. Leenders, R. Citro, A. V. Kimel, R. V. Mikhaylovskiy, B. A. Ivanov, A. D. Caviglia, *Nat. Phys.* **2021**, 17, 1001.
- [12] J. Walowski, M. Müzenberg, *J. Appl. Phys.* **2016**, 120, 140901.
- [13] A. Eschenlohr, U. Bovensiepen, *J. Condens. Matter Phys.* **2017**, 30, 030301.
- [14] P. Němec, M. Fiebig, T. Kampfrath, A. V. Kimel, *Nat. Phys.* **2018**, 14, 229.
- [15] T. Kampfrath, K. Tanaka, K. A. Nelson, *Nat. Photonics* **2013**, 7, 680.
- [16] A. V. Kimel, A. Kirilyuk, P. A. Usachev, R. V. Pisarev, A. M. Balbashov, Th. Rasing, *Nature* **2005**, 435, 655.
- [17] T. Kampfrath, A. Sell, G. Klatt, A. Pashkin, S. Mährlein, T. Dekorsy, M. Wolf, M. Fiebig, A. Leitenstorfer, R. Huber, *Nat. Photonics* **2011**, 5, 31.
- [18] C. Vicario, C. Ruchert, F. Ardana-Lamas, P. M. Derlet, B. Tudu, J. Luning, C. P. Hauri, *Nat. Photonics* **2013**, 7, 720.
- [19] F. Hansteen, A. Kimel, A. Kirilyuk, T. Rasing, *Phys. Rev. Lett.* **2005**, 95, 047402.
- [20] M. Nakajima, A. Namai, S. Ohkoshi, T. Suemoto, *Opt. Express* **2010**, 18, 18260.
- [21] K. Yamaguchi, M. Nakajima, T. Suemoto, *Phys. Rev. Lett.* **2010**, 105, 237201.
- [22] K. Yamaguchi, T. Kurihara, Y. Minami, M. Nakajima, T. Suemoto, *Phys. Rev. Lett.* **2013**, 110, 137204.
- [23] W. Zhang, P. Maldonado, Z. Jin, T. S. Seifert, J. Arabski, G. Schmerber, E. Beaupaire, M. Bonn, T. Kampfrath, P. M. Oppeneer, D. Turchinovich, *Nat. Commun.* **2020**, 11, 4247.
- [24] J. Neu, C. A. Schmuttenmaer, *J. Appl. Phys.* **2018**, 124, 231101.
- [25] *Light Scattering Spectra of Solids* (Ed: G. B. Wright), Springer, Berlin, Heidelberg **1969**.
- [26] P. A. Fleury, R. Loudon, *Phys. Rev.* **1968**, 166, 514.
- [27] R. Loudon, *Adv. Phys.* **1968**, 17, 243.
- [28] S. M. Rezende, A. Azevedo, R. L. Rodríguez-Suárez, *J. Appl. Phys.* **2019**, 126, 151101.
- [29] K. Grishunin, T. Huisman, G. Li, E. Mishina, T. Rasing, A. V. Kimel, K. Zhang, Z. Jin, S. Cao, W. Ren, G.-H. Ma, R. V. Mikhaylovskiy, *ACS Photonics* **2018**, 5, 1375.
- [30] J. Lu, X. Li, H. Y. Hwang, B. K. Ofori-Okai, T. Kurihara, T. Suemoto, K. A. Nelson, *Phys. Rev. Lett.* **2017**, 118, 207204.
- [31] M. F. Thorpe, *J. Appl. Phys.* **1970**, 41, 892.
- [32] S. Azuma, M. Sato, Y. Fujimaki, S. Uchida, Y. Tanabe, E. Hanamura, *Phys. Rev. B* **2005**, 71, 014429.
- [33] M. Le Tacon, G. Ghiringhelli, J. Chaloupka, M. Moretti Sala, V. Hinkov, M. W. Haverkort, M. Minola, M. Bakr, K. J. Zhou, S. Blanco-Canosa, C. Monney, Y. T. Song, G. L. Sun, C. T. Lin, G. M. De Luca, M. Salluzzo, G. Khaliullin, T. Schmitt, L. Braicovich, B. Keimer, *Nat. Phys.* **2011**, 7, 725.
- [34] H. J. Qin, Kh. Zakeri, A. Ernst, J. Kirschner, *Phys. Rev. Lett.* **2017**, 118, 127203.
- [35] C. Kadlec, V. Goian, K. Z. Rushchanskii, P. Kužel, M. Ležaić, K. Kohn, R. V. Pisarev, S. Kamba, *Phys. Rev. B* **2011**, 84, 174120.
- [36] L. Balents, *Nature* **2010**, 464, 199.
- [37] P. Mendels, F. Bert, *C. R. Phys.* **2016**, 17, 455.
- [38] Y. Kohama, H. Ishikawa, A. Matsuo, K. Kindo, N. Shannon, Z. Hiroi, *Proc. Natl. Acad. Sci. USA* **2019**, 116, 10686.
- [39] M. R. Norman, *Rev. Mod. Phys.* **2016**, 88, 041002.
- [40] J. Kollie, R. Moessner, *Annu. Rev. Condens. Matter Phys.* **2019**, 10, 451.
- [41] P. Puphal, M. Bolte, D. Sheptyakov, A. Pustogow, K. Kliemt, M. Dressel, M. Baenitz, C. Krellner, *J. Mater. Chem. C* **2017**, 5, 2629.
- [42] M. Hering, F. Ferrari, A. Razpopov, I. I. Mazin, R. Valentí, H. O. Jeschke, J. Reuther, *npj Comput. Mater.* **2022**, 8, 10.
- [43] Q. Barthélemy, P. Puphal, K. M. Zoch, C. Krellner, H. Luetkens, C. Baines, D. Sheptyakov, E. Kermarrec, P. Mendels, F. Bert, *Phys. Rev. Mater.* **2019**, 3, 074401.
- [44] A. Pustogow, Y. Li, I. Voloshenko, P. Puphal, C. Krellner, I. I. Mazin, M. Dressel, R. Valentí, *Phys. Rev. B* **2017**, 96, 241114.
- [45] D. Watanabe, K. Sugii, M. Shimozawa, Y. Suzuki, T. Yajima, H. Ishikawa, Z. Hiroi, T. Shibauchi, Y. Matsuda, M. Yamashita, *Proc. Natl. Acad. Sci. USA* **2016**, 113, 8653.
- [46] H. Ishikawa, D. Nishio-Hamane, A. Miyake, M. Tokunaga, A. Matsuo, K. Kindo, Z. Hiroi, *Phys. Rev. Mater.* **2019**, 3, 064414.
- [47] D. Boldrin, B. Fåk, E. Canévet, J. Ollivier, H. C. Walker, P. Manuel, D. D. Khalavin, A. S. Wills, *Phys. Rev. Lett.* **2018**, 121, 107203.
- [48] D. V. Pilon, C. H. Lui, T.-H. Han, D. Shrekenhamer, A. J. Frenzel, W. J. Padilla, Y. S. Lee, N. Gedik, *Phys. Rev. Lett.* **2013**, 111, 127401.
- [49] A. C. Potter, T. Senthil, P. A. Lee, *Phys. Rev. B* **2013**, 87, 245106.

- [50] M. Windt, M. Grüninger, T. Nunner, C. Knetter, K. P. Schmidt, G. S. Uhrig, T. Kopp, A. Freimuth, U. Ammerahl, B. Büchner, A. Revcolevschi, *Phys. Rev. Lett.* **2001**, *87*, 127002.
- [51] M. Grüninger, D. van der Marel, A. Damascelli, A. Erb, T. Nunner, T. Kopp, *Phys. Rev. B* **2000**, *62*, 12422.
- [52] J. Lorenzana, G. A. Sawatzky, *Phys. Rev. Lett.* **1995**, *74*, 1867.
- [53] J. D. Perkins, J. M. Graybeal, M. A. Kastner, R. J. Birgeneau, J. P. Falck, M. Greven, *Phys. Rev. Lett.* **1993**, *71*, 1621.
- [54] J. W. Halley, I. Silvera, *Phys. Rev. Lett.* **1965**, *15*, 654.
- [55] Y. Tanabe, T. Moriya, S. Sugano, *Phys. Rev. Lett.* **1965**, *15*, 1023.
- [56] S. J. Allen, Jr., R. Loudon, P. L. Richards, *Phys. Rev. Lett.* **1966**, *16*, 463.
- [57] M. F. Thorpe, R. J. Elliott, *Light Scattering Spectra of Solids* (Eds: G. B. Wright), Springer, Berlin, Heidelberg **1969**, Ch. 2, pp. 199–206.
- [58] D. L. Dexter, *Phys. Rev.* **1962**, *126*, 1962.
- [59] J. W. Halley, *Phys. Rev.* **1967**, *154*, 458.
- [60] L. L. Lohr, Jr., *Coord. Chem. Rev.* **1972**, *8*, 241.
- [61] Y. Tanabe, E. Hanamura, *J. Phys. Soc. Jpn.* **2005**, *74*, 670.
- [62] M. E. Zhitomirsky, A. L. Chernyshev, *Rev. Mod. Phys.* **2013**, *85*, 219.
- [63] J. D. Thompson, P. A. McClarty, D. Prabhakaran, I. Cabrera, T. Guidi, R. Coldea, *Phys. Rev. Lett.* **2017**, *119*, 057203.
- [64] T. Hong, Y. Qiu, M. Matsumoto, D. A. Tennant, K. Coester, K. P. Schmidt, F. F. Awwadi, M. M. Turnbull, H. Agrawal, A. L. Chernyshev, *Nat. Commun.* **2017**, *8*, 15148.
- [65] D. Wulferding, Y. Choi, S.-H. Do, C. H. Lee, P. Lemmens, C. Faugeras, Y. Gallais, K.-Y. Choi, *Nat. Commun.* **2020**, *11*, 1603.
- [66] A. Sahasrabudhe, D. A. S. Kaib, S. Reschke, R. German, T. C. Koethe, J. Buhot, D. Kamenskyi, C. Hickey, P. Becker, V. Tsurkan, A. Loidl, S. H. Do, K. Y. Choi, M. Grüninger, S. M. Winter, Z. Wang, R. Valentí, P. H. M. van Loosdrecht, *Phys. Rev. B* **2020**, *101*, 140410.
- [67] L. Pan, S. K. Kim, A. Ghosh, C. M. Morris, K. A. Ross, E. Kermarrec, B. D. Gaulin, S. M. Koohpayeh, O. Tchernyshyov, N. P. Armitage, *Nat. Commun.* **2014**, *5*, 4970.
- [68] S. M. Winter, K. Riedl, P. A. Maksimov, A. L. Chernyshev, A. Honecker, R. Valentí, *Nat. Commun.* **2017**, *8*, 1152.
- [69] Z. Wang, S. Reschke, D. Hüvonen, S.-H. Do, K.-Y. Choi, M. Gensch, U. Nagel, T. Rööm, A. Loidl, *Phys. Rev. Lett.* **2017**, *119*, 227202.
- [70] K. Kozuki, T. Nagashima, M. Hangyo, *Opt. Express* **2011**, *19*, 24950.
- [71] A. Togo, F. Oba, I. Tanaka, *Phys. Rev. B* **2008**, *78*, 134106.
- [72] A. Togo, I. Tanaka, *Scr. Mater.* **2015**, *108*, 1.
- [73] G. Kresse, J. Hafner, *Phys. Rev. B* **1993**, *47*, 558.
- [74] G. Kresse, J. Furthmüller, *Phys. Rev. B* **1996**, *54*, 11169.
- [75] G. Kresse, J. Furthmüller, *Comput. Mater. Sci.* **1996**, *6*, 15.
- [76] S. Toth, B. Lake, *J. Condens. Matter Phys.* **2015**, *27*, 166002.